EEG-based visual deviance detection in freely behaving mice

Renate Kat[a], Berry van den Berg[b], Matthijs JL Perenboom[c], Maarten Schenke[d], Arn MJM van den Maagdenberg[c,d], Hilgo Bruining[e], Else A Tolner[c,d*], Martien JH Kas[a *]

[a]Groningen Institute for Evolutionary Life Sciences (GELIFES), University of Groningen, Nijenborgh 7, 9747 AG, Groningen, the Netherlands, r.kat@rug.nl, m.j.h.kas@rug.nl

[b]Faculty of Behavioural and Social Sciences, Cognitive Neuroscience, Department of Experimental Psychology, University of Groningen, Grote Kruisstraat 2/1, 9712 TS, Groningen, the Netherlands, berry.van.den.berg@rug.nl

[c]Department of Neurology, Leiden University Medical Center, Albinusdreef 2, 2300 RC, Leiden, the Netherlands, M.J.L.Perenboom@lumc.nl, A.M.J.M.van_den_Maagdenberg@lumc.nl, E.A.Tolner@lumc.nl

[d]Department of Human Genetics, Leiden University Medical Center, Einthovenweg 20, 2300 RC, Leiden, the Netherlands.

[e]Department of Child and Adolescent Psychiatry, Amsterdam University Medical Center, University of Amsterdam, Postbus 7057, 1007 MB, Amsterdam, the Netherlands, h.bruining@amsterdamumc.nl

*These authors have contributed equally to this work

Corresponding author:

Prof. Dr. MJH Kas; Groningen Institute for Evolutionary Life Sciences (GELIFES), University of Groningen, Nijenborgh 7, 9747 AG Groningen, The Netherlands m.j.h.kas@rug.nl

Abbreviations ERP: event related potential; MMN: mismatch negativity; TFR: time-frequency reponse; V1: primary visual cortex; VEP: visual evoked potential

Abstract

The mouse is widely used as an experimental model to study visual processing. To probe how the visual system detects changes in the environment, functional paradigms in freely behaving mice are strongly needed. We developed and validated the first EEG-based method to investigate visual deviance detection in freely behaving mice. Mice with EEG implants were exposed to a visual deviant detection paradigm that involved changes in light intensity as standard and deviant stimuli. By subtracting the standard from the deviant evoked waveform, deviant detection was evident as bi-phasic negativity (starting around 70 ms) in the difference waveform. Additionally, deviance-associated evoked (beta/gamma) and induced (gamma) oscillatory responses were found. We showed that the results were stimulus independent by applying a "flip-flop" design and the results showed good repeatability in an independent measurement. Together, we put forward a validated, easy-to-use paradigm to measure visual deviance processing in freely behaving mice.

Keywords

visual processing, mismatch negativity, sensory processing deficits

1. Introduction

The experiments by Hubel and Wiesel on direction selectivity of neurons in the cat visual cortex (Hubel, 1959; Hubel & Wiesel, 1968) have pioneered a growing scientific field on the visual system and its processing abilities. Since then, the mouse is a widely used animal model to investigate visual processing (Baker, 2013). One important reason is that mice are particularly suitable for genetic modification, such as the use of advanced genetically encoded tools for neuroimaging and neuromodulation that allow unravelling of neuronal network dynamics (Warden et al., 2014). Moreover, transgenic mouse models allow to examine the role of specific cell types or neuronal populations (Sohya et al., 2007; Hamm and Yuste, 2016), as well as to study altered visual processing in the context of human psychiatric disorders (Zhang et al., 2017; Hamm et al., 2020; Perenboom et al., 2020). However, visual processing has hardly been studied in awake, freely behaving mice, as typically head-fixation is used to ensure that visual stimuli reach the eye (Montijn et al., 2016; Carrillo-Reid et al., 2019; Fournier et al., 2020). Assessing measures of visual processing in freely moving mice requires a behavioural setup in which animals are constantly exposed to visual stimuli in their environment irrespective of their bodily position.

Detecting changes in the environment is an important function of sensory systems. The brain can shift attention to changes in the environment via either a passive reduction in the response to redundant stimuli, or an active memory-based increased response to unexpected, or deviant, stimuli (Garrido et al., 2009). The representation of deviance detection in the EEG signal has also been called mismatch negativity (MMN; May et al., 1999). Deficits in deviance detection have been associated with various neuropsychiatric disorders, mainly schizophrenia (Näätänen et al., 2014; Tada et al., 2019). Visual deviance

detection has gained substantially less attention compared to auditory deviance detection and has only twice been studied in rodents (Hamm and Yuste, 2016; Vinken et al., 2017). While these studies were able to assess visual deviance detection, the animals were required to be head-fixated.

Here we set out to develop a novel paradigm to measure deviance-induced differences in visual evoked potentials (VEPs) in freely behaving mice. Based on MMN oddball concepts used in the context of auditory deviance detection (Harms et al., 2016), our visual deviant detection paradigm involves changes in light intensity as standard and deviant stimuli. In order to use the measured EEG waveform difference features for 'deviance detection', the paradigm needs to comply with three principal criteria. First, the paradigm should be able to elicit a *robust deviance response* as measured through the difference between the deviant versus standard VEP responses. Second, the deviance response needs to be *stimulus-independent,* meaning that the same response difference is found when using either of the two stimuli - in our case increases versus decreases in light intensity – as deviant. Third, the VEP deviance effect needs to be repeatable in an independent measurement within the same subject (*repeatability*). After satisfying the three criteria based on VEP waveforms, characteristics of the frequency responses for the paradigm were explored to gain insight in visual deviance-induced oscillatory activity. In addition, the influence of the repeated light stimulation was explored by assessing how the strength of the observed deviance detection changed with increasing number of standards preceding a deviant.

2. Materials and Methods

2.1 Mice

Male C57BL/6J mice (n=13) were used to implement and validate the newly developed visual deviance detection paradigm. Animals were single-housed in individually ventilated cages for at least one week prior to surgeries and maintained on a 12:12 light-dark cycle with *ad libitum* access to food and water. All experiments were approved by the Animal Experiment Ethics Committee of Leiden University Medical Center and were carried out in accordance with ARRIVE guidelines and EU Directive 2010/63/EU for animal experiments. All efforts were made to minimize discomfort of the experimental animals.

2.2 EEG implantation surgery

Stereotactic EEG electrode implantation surgery was performed in mice at the age of 2 months. Under isoflurane anaesthesia (1.5%, in oxygen-enriched air), three silver (Ag) ball-tip electrodes were implanted epidurally above the right prefrontal cortex (bregma +2.6 mm anterior, -1.6 mm lateral) and the right and left primary visual cortex (V1; bregma -3.5 mm posterior, +/- 3.0 mm lateral). The relatively lateral V1 position was chosen since multiple studies indicate a role for the visual extra-striate areas (which are located more laterally on the occipital cortex) in the visual deviance detection (reviewed in: Kimura, 2012; Vinken et al., 2017). Two epidural platinum electrodes were placed above cerebellum to serve as reference and a ground electrode, respectively. Electromyogram (EMG) electrodes were placed on top of the neck muscles to record muscle activity. Light-activated bonding primer and dental cement (Kerr optibond / premise flowable, DiaDent Europe, Almere, the Netherlands) were used to attach electrodes to the skull. Post-operative pain relief was achieved by a subcutaneous injection of Carprofen (5 mg/kg). EEG recordings started after a 14-day recovery period.

2.3 EEG and VEP recordings

Tethered EEG recordings were performed in a Faraday cage in which animals were connected to the recording hardware via a counterbalanced, low-torque custom-build electrical commutator. Signals were three times pre-amplified, band-pass filtered (0.05 to 500 Hz), then amplified 1200 times and thereafter digitized (Power 1401, Cambridge Electronic Devices, Cambridge, UK) at a sampling rate of 5000 Hz. For the recording of VEPs, mice were placed inside a computer-controlled custom-built LED-illuminated sphere in which tethered mice were able to move freely (Van Diepen et al., 2013). The sphere (30 cm diameter) was coated with high-reflectance paint that spread light produced by a ring of white monochromatic LEDs at the top of the sphere around an opening for the swivel. A baffle prevented the mice from looking directly into the LEDs. After connecting mice to the setup in the sphere, animals were allowed to habituate for at least 10 min. Mice were tested once in an input-output paradigm and twice in an oddball paradigm, all on separate days. The input-output paradigm, in which a train of light flashes of increasing intensity was presented to the animals, was performed to determine VEP signal quality. 60 flashes of 1 ms with increasing light intensity between ~0.4 to 1.1 μW/cm^2/nm were presented at 2 Hz, and 5 flashes of increasing intensity between ~1.4 to 2.2 μW/cm^2/nm at 0.5 Hz. The paradigm was repeated 50 times with 20 s rest in-between blocks.

2.4 Visual oddball paradigm

To measure visual deviance detection, a light intensity-based oddball paradigm with decreases and increases in light intensity was developed (Fig. 1). To ensure stable levels of light-adaptation before onset of the oddball sequence, the paradigm started with 10 min of constant light of medium intensity (0.15 μW/cm^2/nm). Subsequently a 7-minute sequence started in which 300-ms pulses of increased (1.7 μW/cm^2/nm) or decreased

light intensity (0.02 μW/cm^2/nm) stimuli were interspersed by a 500-ms inter-stimulus interval of the 0.15 μW/cm^2/nm constant light intensity (Fig. 1). The constant level of light in between the sequence of standard and deviant stimuli was used to prevent occurrence of dark adaptation between stimuli. The intensities of increases (1.7 μW/cm^2/nm) and decreases (0.02 μW/cm^2/nm) were chosen based on VEP amplitudes in the grand average input-output curve in such a way that the amplitude change from decrease to ISI level was the same as the amplitude change from ISI to increase level. The stimulus duration of 300 ms was based on earlier visual MMN studies that used stimulus durations between 80 and 500 ms, in humans (Stagg et al., 2004; Kimura et al., 2010; Sulykos and Czigler, 2014) and rodents (Hamm and Yuste, 2016; Vinken et al., 2017). Deviant stimuli were semi-randomly spread through the sequence, with the constraint of a minimum of two standard presentations before the next deviant. The first stimulation block in the paradigm contained 500 stimuli, 473 (87.4%, the standard) of which were intensity increases and 63 (12.6%, the deviant) of which were light intensity decreases. After this block, the paradigm (including the 10 minutes constant light at the start) was repeated with a swap of standard and deviant stimulus type. This so called 'flip-flop' paradigm allowed for assessment of differences between standard and deviant stimuli irrespective of stimulus type (Harms et al., 2016), in our case increased *vs* decreased light intensity. The visual oddball paradigm was performed twice for every animal on separate days. The order of the first and second recording was counterbalanced over the morning (1st half of the light phase) and the afternoon (2nd half of the light phase).

2.5 Analysis

No animals had to be excluded on the basis of low signal quality found in the input-output paradigm. For two animals, positive-negative inverted signals were evident on one of the

visual cortex electrodes (once right V1 and once left V1); these electrodes were excluded from analysis. Next, recordings were manually checked to exclude recording periods with artefacts, as well as periods of sleep, as deviance detection is known to be attenuated or even absent in non-REM sleep (Sculthorpe et al., 2009). For sleep detection, recordings were first screened for the presence of periods where an infrared motion detector did not pick up non-specific locomotor activity. If periods without locomotor activity were present during stimulus presentation, they were checked for the presence of non-REM sleep, as defined by high amplitude delta (<4 Hz) waves, so called slow waves, in the frontal EEG signal in combination with an absence of activity in the EMG signal. Two recordings which contained periods of sleep were excluded from analysis (both being the first recording of the animal).

Data pre-processing was performed in Matlab (Versions 2018a & 2018b, MathWorks, Natick, MA, USA). EEG data were low-pass filtered at 70 Hz with a fourth order Butterworth filter. For evoked potential waveform analysis, VEPs were extracted from the data of each recording electrode from 50 ms before until 300 ms after stimulus onset. Subsequently, VEPs were grouped into deviant and standard stimuli, irrespective of being a light intensity increase or a light intensity decrease. Within those two categories, all VEPs were averaged, and baseline corrected, using a latency window that ranged from -50 to 0 to ms prior to the change in light intensity. Difference waves were calculated by subtracting the standard from the deviant VEP. A comparison between the difference waves of the right and left V1 electrode (using cluster-based permutation analysis) did not reveal any time windows of significant differences (data not shown). In subsequent analyses VEPs from the right and left electrode were averaged.

For analysis of time-frequency responses (TFRs), single trial data (i.e. from a single stimulation; either a standard or deviant) were extracted from the EEG signal from 1 s

before to 1.5 s after stimulus onset. For time-frequency analysis, the data was low-pass filtered at 150 Hz. Like with the VEP analysis, trials were grouped into standards and deviants irrespective of the stimulus being a light increase or decrease. Using the FieldTrip toolbox for EEG/MEG-analysis (Oostenveld et al., 2011; Donders Institute for Brain, Cognition and Behaviour, Radboud University, the Netherlands), Hanning window convolution was performed with 5ms time windows. Frequencies were extracted from 4 - 150 Hz with 1-Hz linear steps. The number of cycles increased from 2 to 10 with increasing frequency. Next, power was converted to a log10 scale and an absolute baseline correction was performed using a window from 200 until 100 ms before stimulus onset as the baseline. This window was chosen to avoid including stimulus related activity that would be smeared (in time) due the width of the Hanning window. The average time-frequency map of standard trials was subtracted from the average time-frequency map of deviant trials. Additionally, to assess non-phase-locked TFRs, per condition the *average* VEP response was subtracted from individual trials in the time domain before performing the same time-frequency analysis as described above (Stothart and Kazanina, 2013).

2.6 Statistics

To test whether deviance detection was significantly different from zero for both the VEPs and TFRs, cluster-based permutation analysis was used as previously described (Maris and Oostenveld, 2007). In short, dependent *t*-test statics were obtained for every time- (0.2-ms steps) or time-frequency point (5-ms to 1-Hz steps) and were clustered over time (and frequency) along adjacent points that reached above the *t*-value threshold corresponding to an alpha-level of 0.05. The sum of all *t*-values in a cluster was used as the cluster statistic. To assess significance of these clusters, a 'null' distribution was

created by performing 1000 random permutations with the individual animal difference waves/maps and zero. Cluster statistics were extracted for every permutation in the same manner as described above. Both the largest positive and the largest negative cluster from each permutation were used to create two distributions. Clusters in the actual data were considered significant when exceeding the 97.5-percentile threshold for cluster size in either the positive or negative distribution.

Comparable procedures were used to compare VEP features between right and left electrodes, light intensity increases and decreases, and first and second recordings. However, in these cases permutations were performed by randomly exchanging the data between the two conditions in the comparison. Clusters were reported when $p<0.2$, were $p<0.05$ was considered significant. Cluster-based permutation analysis does not have a good level of precision for finding exact on- and off-sets, therefore borders of the time, as well as time-frequency, windows of reported clusters should be interpreted carefully (Sassenhagen and Draschkow, 2019). To explore the effects of the number of standards since the last deviant, in other words the number of preceding standards, on neural responses (both VEPs and TFRs) and deviance detection amplitude, linear mixed modelling was performed (Bates et al., 2015; Kuznetsova et al., 2017). Models were estimated and analysed using package lme4 (RStudio, version 1.2.5042 (R-version 4.0), Boston, MA, USA; lme4 package version 1.1-23) and lmerTest. Using mixed models allowed taking into account the number of individual trials that contribute to a condition (as opposed to calculating the unpoled means per subject, per condition, losing this type of information). The VEP waveform mean amplitudes were extracted from each individual trial in the latency windows that were found to be significant clusters in the evoked potential analysis, resulting in two separate models for an early (40 to 60 ms) and a late (70 to 150 ms) latency window. Similarly, the mean frequency power from

each of the TFR clusters (across frequencies and time) that were found to be significant was also extracted. These mixed modelling analyses should be viewed as exploratory only; by using a time and frequency window defined by an earlier statistical analysis, we are increasing type I error-rate by an unknown amount (Kriegeskorte et al., 2009).

The amplitude of the VEP waveforms and power of the TFRs were inspected as a function of the number of trials since the last deviant, for both standards and deviants, and light increases and decreases. Fewer observations were available for increasing number of trials since the last deviant. A model was constructed with model selection based on Akaike Information Criterion (AIC) to control for type I error rate, with statistical significance assessed using Satterthwaite estimation of effective degrees of freedom (pooled degrees of freedom) (Matuschek et al., 2017).

$$\begin{aligned} \mathrm{mV_n} \mid cluster\ power_n \\ &= \beta_{0.\mathrm{j}} + \beta_1 \#\mathrm{trials_{j[n]}} + \beta_2 \mathrm{stimulus_{j[n]}} + \beta_3 \mathrm{light_n} + \beta_4 \#\mathrm{trials_n}.\mathrm{stimulus}_n \\ &+ \beta_5 \#\mathrm{trials_n}.\mathrm{light}_n + \beta_6 \mathrm{stimulus_n}.\mathrm{light}_n + \beta_6 \#\mathrm{trials_n}.\mathrm{stimulus}_n.\mathrm{light}_n + \epsilon_\mathrm{n} \end{aligned}$$

In this formula, for each trial n, the VEP and TFR amplitudes were described by an intercept β_0 which indicates a random intercept per animal, β_1 which indicates the number of trials since last deviant (1-30), β_2 which relates to whether the trial was a deviant or a standard and β_3 which indicates whether the trial was a light increase or decrease. Finally, $\beta_{4\text{-}7}$ are the interactions between those terms and ϵ_n is the residual error term.

VEP figures were constructed in GraphPad Prism (Version 8, GraphPad Software, San Diego, CA, USA). Figures of the TFR were constructed in Matlab. Figures of the mixed linear modelling data were constructed in RStudio. All data and analysis code (R and Matlab) is available on the OSF data repository (www.osf.io/6bhwf/).

3. Results

3.1 Visual deviance detection can be assessed in freely behaving mice

For the development of the visual deviance detection paradigm for freely behaving mice, we designed an oddball paradigm with sequences of 300-ms white light pulses of increased (1.7 μW/cm^2/nm) or decreased (0.2 μW/cm^2/nm) light intensity, interspersed by a 500-ms interstimulus interval at constant light of intermediate intensity (0.15 μW/cm^2/nm, Fig. 1). Deviant stimuli (63 of 500 stimuli, 12.6%) were semi-randomly spread throughout the sequence with the constraint of a minimum of two standard presentations before the next deviant. In the paradigm both increases and decreases in light intensity were presented once as standard and once as deviant ('flip-flop' paradigm; Harms et al., 2016, Fig. 1). The paradigm was presented twice, on separate days. For the first analysis, VEP responses were averaged for, respectively, all standard and deviant stimuli, regardless of being a response to a light increase or light decrease. VEPs recorded from the right and left primary visual cortex (V1), and the first and the second measurement were combined.

Visual inspection of the averaged VEPs revealed a clear distinction between standard and deviant waveforms (Fig. 2A). Both for deviant and standard stimuli, VEPs showed an initial N1 negativity around 30 ms after stimulus onset, followed by a broad positivity between ~50 and ~150 ms. Compared to the response to standard stimuli, the deviant N1 deflection was slightly broadened, while the later broad positivity was of lower amplitude than observed for the standard response. Consequently, the difference wave, computed by subtracting the standard from the deviant response, consisted of a bi-phasic negative component, between ~35 and ~150 ms, with a maximum peak amplitude of -0.048 ± 0.027 mV (Fig. 2B). Cluster-based permutation analysis revealed two

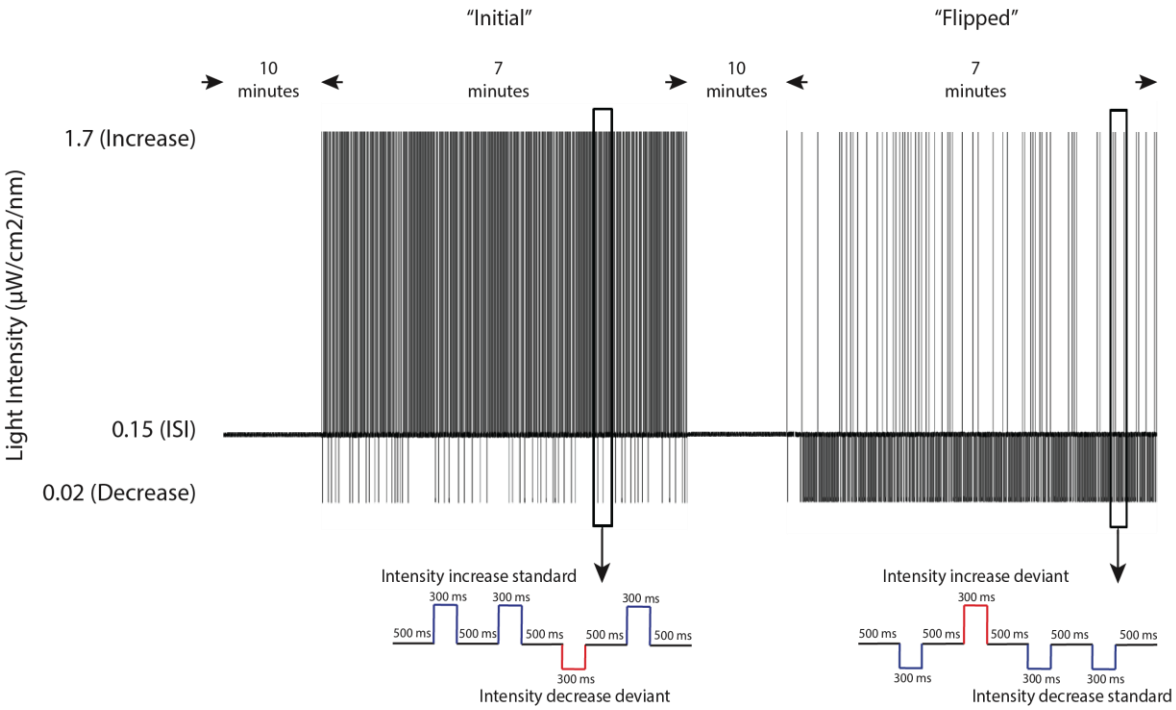

Figure 1 Graphical representation of the light-intensity oddball paradigm used for visual deviance detection in freely behaving mice. Mice were presented with an oddball paradigm with increases (1.7 µW/cm²/mm) and decreases (0.02 µW/cm²/mm) in light intensity as stimuli, with intermittent intermediate intensity levels (0.15 µW/cm²/mm). The paradigm was presented as a 'flip-flop' in which the "initial" presentation with intensity increase standards and intensity decrease deviants (left), was followed by a "flipped" presentation with intensity decrease standards and intensity increase deviants (right). Initial and flipped stimulation blocks lasted ~ 7 min each. Before the initial stimulation block and in between the initial and flipped stimulation blocks, 10 min of constant intermediate light (0.15 µW/cm²/nm) was presented. For the analysis, standards of increased intensity were compared to deviants of increased intensity, and standards of decreased intensity are compared to deviants of decreased intensity.

deviance-associated components. The early negative component in the difference wave, ~35-60 ms after stimulus onset, showed a trend towards significance (p=0.072), whereas the late negative component, ~70-150 ms after stimulus onset, was significantly different from zero (p=0.004). Our visual oddball paradigm thus meets the first criterion of *yielding a robust deviance response*, as a significant difference in the response to deviant compared to standard light stimuli could be assessed from VEPs recorded from V1 in freely

behaving mice. Compared to the V1 EEG recordings, the oddball paradigm elicited no apparent VEP responses at the prefrontal electrode, nor a distinguishable difference wave (data not shown), indicating specificity of the test paradigm to the visual system.

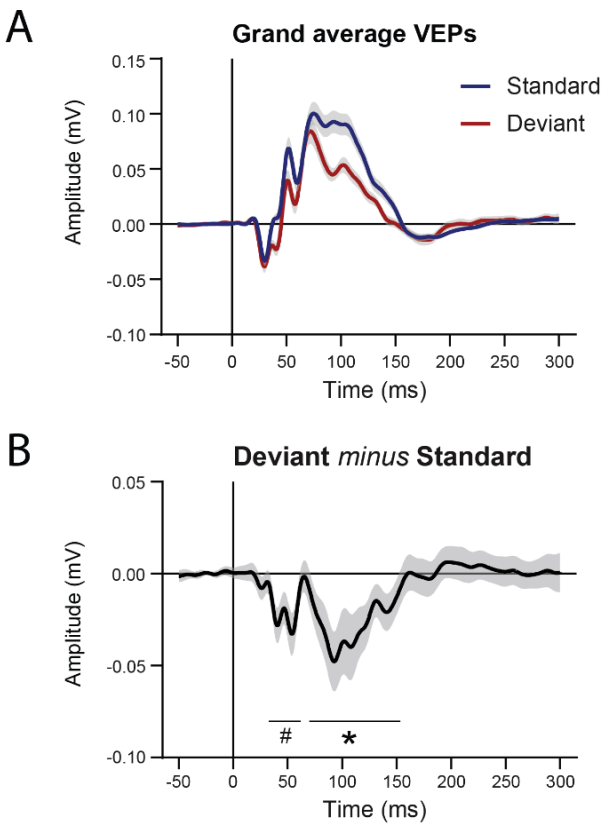

Figure 2 Visual deviance detection in the visual evoked potential responses to an intensity oddball paradigm in freely behaving mice. (A) Grand average VEP waveforms in response to standard and deviant stimuli. Responses were averaged for, respectively, all standard or all deviant stimuli, independent of the standard or deviant representing a stimulus of increased or decreased light intensity. Responses of the right and left V1, as well as the first and second recording were combined. Data are presented as mean ± standard error of the mean (SEM). **(B)** Deviant minus standard difference wave for the combined 'intensity increase' and 'intensity decrease' deviants and standards. Data are presented as mean ± 95% confidence interval. n = 13, *p<0.01, #p<0.1.

3.2 Visual deviance detection in the late VEP component is stimulus-independent

To meet the deviance detection criterion of stimulus independency, the difference between VEP responses to standard and deviant stimuli of intensity increases and intensity decreases should contain similar components. Visual inspection of the standard and deviant VEP waveforms (averaged over the responses from V1 left and right, and the two different recording days) revealed different features in the context of intensity

increase or decrease stimuli, in particular with respect to the early latencies. Specifically, the VEP in response to an intensity increase, for both standard and deviant stimuli, contained additional early latency components between 20 and 60 ms that were not evident in the VEP in response to an intensity decrease (Fig. 3A).

While the early components of standard and deviant VEP waveforms for light increases and decreases differed, when subtracting the standard from the deviant response for stimuli of the same light change (i.e. increase or decrease), the deviant-minus-standard difference waves were remarkably similar for both light intensity changes with respect to the late component around 100 ms (Fig. 3B). The late component of the difference wave, at a latency range of ~70-150 ms, was significantly different from zero for both the intensity increase ($p=0.04$) as well as the intensity decrease responses ($p=0.032$). On the other hand, the early component of the difference wave was only evident in the difference wave of an intensity increase ($p=0.024$). For the difference wave of the intensity decrease responses, the shape of the early component was visible but did not differ in amplitude from zero (cluster-based permutation analysis found two clusters due to the return to baseline: $p=0.528$ and $p=0.602$, a one-sample *t*-test on the mean amplitude of the whole latency window 43-62 ms: $p=0.071$). After 150 ms, the difference waves from the intensity increase and decrease responses showed slow shifts in opposite direction which was most evident beyond the ~200 ms latency range of the original VEPs (intensity increase: $p=0.034$; intensity decrease: $p=0.002$). When comparing the features of the light increase and the light decrease difference waves directly, a trend-significant difference was found for the early component (~20-60 ms, $p=0.054$), but no differences were found for the late component ($p=0.72$). In addition, outside the identified window of deviance detection (~30-150 ms), a significant difference between the intensity increase and decrease difference waves was found for

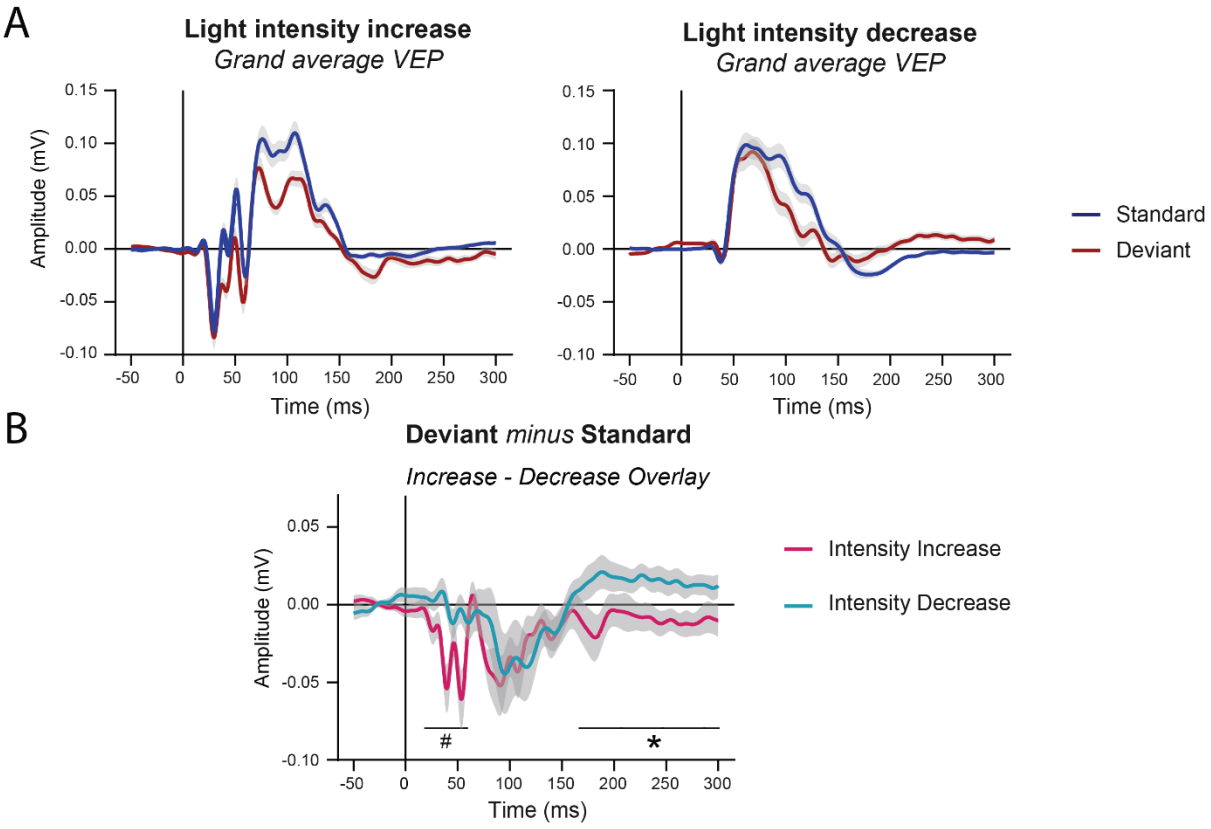

Figure 3 Visual deviance detection in the visual evoked potential responses to light pulses of increased or decreased intensity. (A) The VEP waveforms for, respectively, 'intensity increase' (left) and 'intensity decrease' (right) deviants and standards. Data are presented as mean ± standard error of the mean (SEM). **(B)** Overlay of the intensity increase and intensity decrease difference waves. The early negative wave component between 20-60 ms is present only in the difference wave for intensity increase deviants and standards, the late negative wave component around 100 ms is present in both difference waves. A trend level difference between the two difference waves is observed for the early latencies between 20-60 ms. For latencies between 170-300 ms, the waveforms of the intensity increase and decrease difference waves are significantly different. Data are presented as mean ± 95% confidence intervals. Responses were averaged for right and left V1, as well as the first and second recording. n = 13, *p<0.01, #p<0.1.

the additional late component between ~170-300 ms (p=0.004). In conclusion, although the early latency component was more pronounced in light intensity increase difference waves, the late negative component at ~100 ms was highly similar for the responses to light intensity increases and decreases. With the use of this component of the deviant-

minus-standard difference waves, our visual deviance detection paradigm thus satisfies our second criterion of *stimulus independency*.

The comparison of the intensity increase and decrease responses also revealed, perhaps not surprisingly, that the 'off-response' to an intensity increase – in essence being an intensity decrease – showed a VEP similarly shaped as the 'on-response' of the intensity decrease and vice versa (Supplementary Fig. 1). Increases and decreases in light intensity thus seemed to be processed as *shifts* in light intensity rather than as flashes of *different* intensities. The on- and off-responses to a light increase showed slightly higher amplitudes compared to the on- and off-responses to a light decrease. The chosen magnitude of the intensity shifts, which was larger for increases than decreases (i.e. a shift from 0.15 to 1.7 compared to 0.15 to 0.02 $\mu W/cm^2/mm$), was selected based on tests with a 1-ms flash VEP paradigm that showed an equal amplitude difference for both increase and decrease intensities compared to the VEP amplitude response to the ISI intensity. However, in the deviant paradigm the larger intensity shifts still evoked a slightly higher amplitude response. As the latencies of all identified deviance detection components fall within the 300-ms duration of the light stimuli, these off-responses do not affect our deviance detection.

3.3 Visual deviance detection shows repeatability in an independent measurement

Our third criterion for a deviance detection paradigm concerns repeatability of the outcome in independent measurements. To assess this, each animal was subjected to the visual oddball paradigm twice on two separate days. Using cluster-based permutation analysis, no differences between the first and second recording were observed for either the standard VEPs, deviant VEPs or difference waves for the combined responses to intensity increases and decreases (Fig. 4). Only one small cluster with a trend towards

392 significance was found for the standard VEP (~100-110 ms, p=0.066). These outcomes
393 indicate that our visual oddball paradigm has a good *test-retest reliability* and therefore
394 also meets the third criterion.

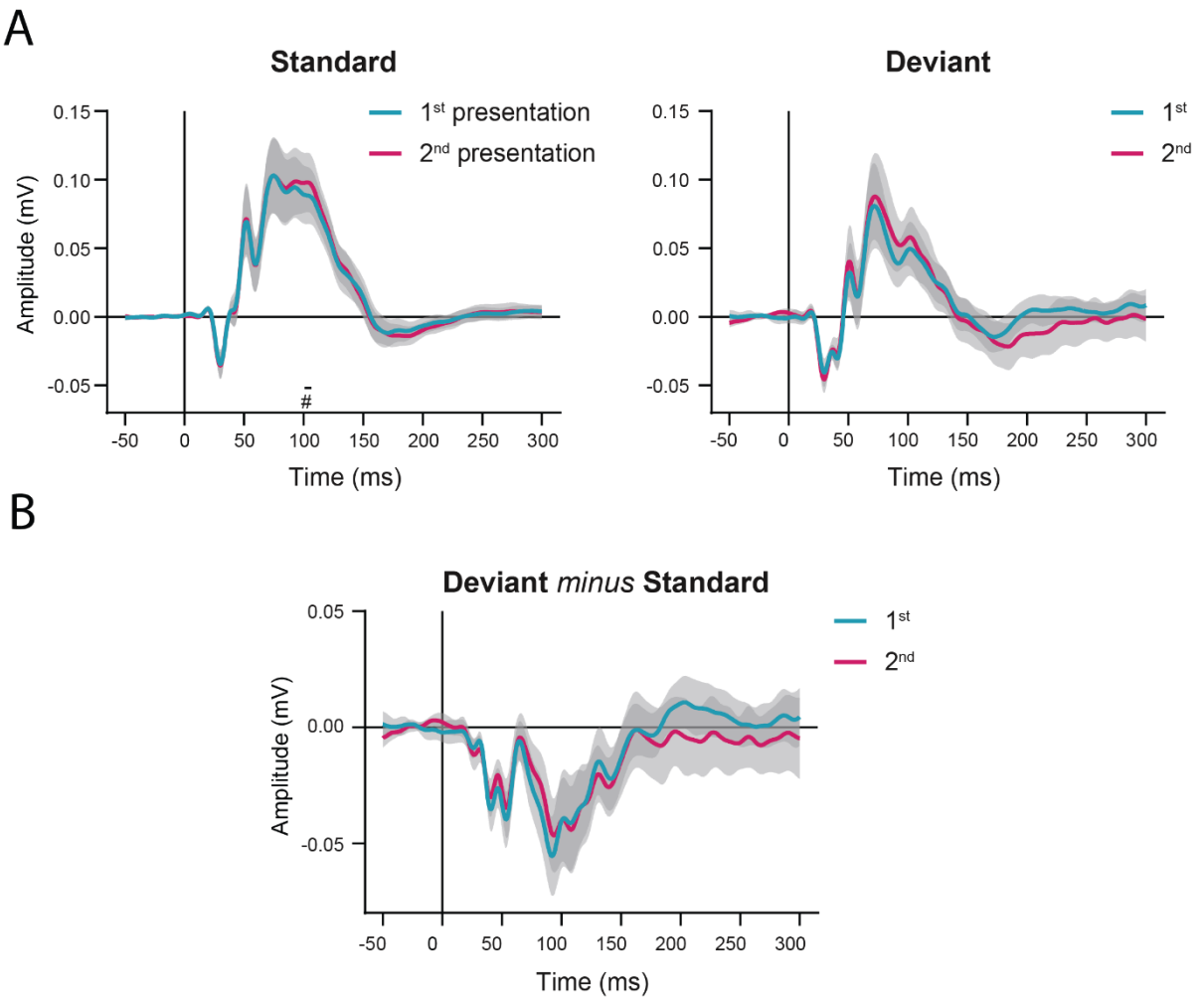

395

396 **Figure 4. Comparison of the visual evoked potential responses from the 2 independent**
397 **measurements.** The same light intensity oddball paradigm was presented to all mice twice, on separate
398 days (i.e. 1st and 2nd presentation). **(A)** VEPs in response to standard and deviant stimuli, averaged for,
399 respectively, the 1st and the 2nd presentation. **(B)** Overlay of the deviant minus standard difference waves.
400 n = 11, data are presented as mean ± 95% confidence interval. Cluster-based permutation analysis did not
401 reveal any significant differences between the 1st and the 2nd presentation.

402 *3.4 Visual deviance detection is also evident from the light-triggered time-frequency*
403 *response*

In addition to examining VEP waveform features from the deviant-standard difference waves, we analysed the EEG TFR. Human studies showed that visual deviance detection has oscillatory components that are not phase-locked to the stimulus and would therefore cancel out when averaging over trials that is part of classical event-related potential (ERP) analysis (Stothart and Kazanina, 2013). TFRs are time-locked, but in contrast to ERP waveforms, not necessarily phase-locked to the stimulus and can therefore give a more complete picture of stimulus-associated activity. Visual inspection of the frequency spectra in response to standards and deviants revealed activity in several frequency ranges. The EEG response to standard stimuli – combined for intensity increases and decreases – showed an apparent increased power for the beta-lower gamma (~20-40 Hz, labelled with '1' in Fig. 5A) and the gamma range (~50-100 Hz, labelled with '2' in Fig. 5A) at a latency between ~20 and ~70 ms after stimulus onset. In addition, a broad increase in power was seen for the theta range (~4-9 Hz, labelled with '3' in Fig. 5A), evident from stimulus onset to a latency of ~200 ms. While the TFR to deviant stimuli showed an overall comparable pattern (Fig. 5A), comparison between deviant and standard TRFs in a deviant minus standard heatmap revealed multiple clusters with significantly different frequency components (Fig. 5A). Most evident was a cluster between ~20-120 ms, indicating increased EEG power in the range from ~10-70 Hz in response to deviants ($p=0.022$, labelled with 'A' in Fig. 5A). This cluster seemed to be the result of a combination of an altered shape of the beta/gamma response (labelled with '1') to the deviant compared to the standard stimuli, as well as an additional deviant response in the alpha/beta band (~10-20 Hz, labelled with '4' in Fig. 5A) which was not evident in the response to the standard. The gamma response (~50-100 Hz) contained less power in response to deviant compared to standard stimuli ($p=0.048$, labelled with 'B' in Fig. 5A). Lastly, increased EEG power in

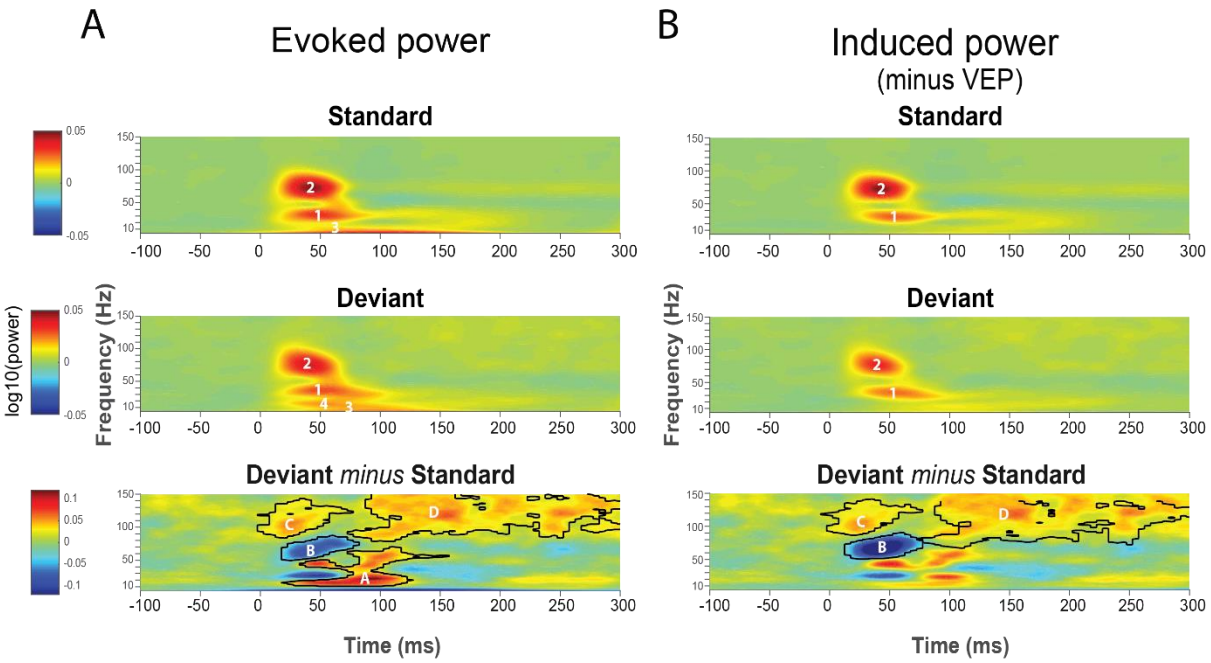

Figure 5. Visual deviance detection in the time-frequency response. Panels show clusters of the power of both overall evoked oscillatory activity **(A)**, as well as induced oscillatory activity **(B)** in the visual deviance detection paradigm. To isolate induced oscillatory activity, the averaged waveform was subtracted from each individual trial before running a time-frequency analysis. From top to bottom panel time-frequency responses to standard stimuli, deviant stimuli, and a deviant minus standard difference plot are shown. TFRs were obtained by performing Hanning-window convolution 4-150 Hz with 5 ms time steps. Absolute baseline-correction was performed using -0.2 - -0.1 ms as the baseline. TFRs to light increases and decreases, the right and left V1 as well as and second recording were averaged. Y-axis lower cut-off is 4 Hz. In the difference plot, significant ($p<0.05$) time-frequency clusters are outlined. n=13.

the high gamma range (~80-150 Hz) was seen in response to the deviant compared to the standard, both shortly following stimulus onset between ~0-60 ms ($p=0.036$, labelled with 'C' in Fig. 5A) and in a later window between ~90 and ~300 ms ($p=0.002$, labelled with 'D' in Fig. 5A).

Oscillatory activity can be divided into evoked power, which is the direct frequency representation of the VEP waveform response, and induced power, which is the oscillatory activity that is non-phase-locked to the stimulus and thus not found in the VEP waveforms (Jones, 2016). To asses which oscillatory clusters in our analysis

represented evoked power and which clusters represented induced power, the time-frequency analysis was also ran after subtracting the average VEP waveform from every single trial per condition (Park et al., 2018). Clusters 3 and 4 in the TFR and cluster A in the difference plot were no longer present after this analysis (Fig. 5B) and thus represent evoked power. On the other hand, clusters 1 and 2 in the TFR and clusters B, C and D in the difference plot were still present after running time-frequency analysis on mean-subtracted data and represent the power of induced oscillatory activity. With our visual oddball paradigm in freely behaving mice, deviance detection was thus not only reflected in the VEP waveforms, but also in evoked as well as induced power in the EEG time-frequency responses.

3.5 Higher numbers of standards preceding a deviant strengthen visual deviance detection

In light of the ongoing debate about the role of adaptation to the repeatedly presented standards in deviance detection paradigms (Garrido et al., 2009; Grimm et al., 2016), we assessed whether stimulus history influenced our VEP-based visual deviance detection. We explored whether the deviance detection amplitude (VEP- and TRF-based) changed with varying numbers of standards preceding the deviant. In addition, we assessed whether this was potentially also affected by the stimulus types, i.e., an intensity increase or decrease. The mean amplitude and oscillatory power of standard and deviant VEPs and TFRs were extracted from each trial, for both the cluster-based defined early (40-60 ms) and late (70-150 ms) latency windows rounded to the nearest ten, and the identified gamma (B, ~50-100 Hz) and high gamma (C and D, ~80-150 Hz) induced frequency clusters.

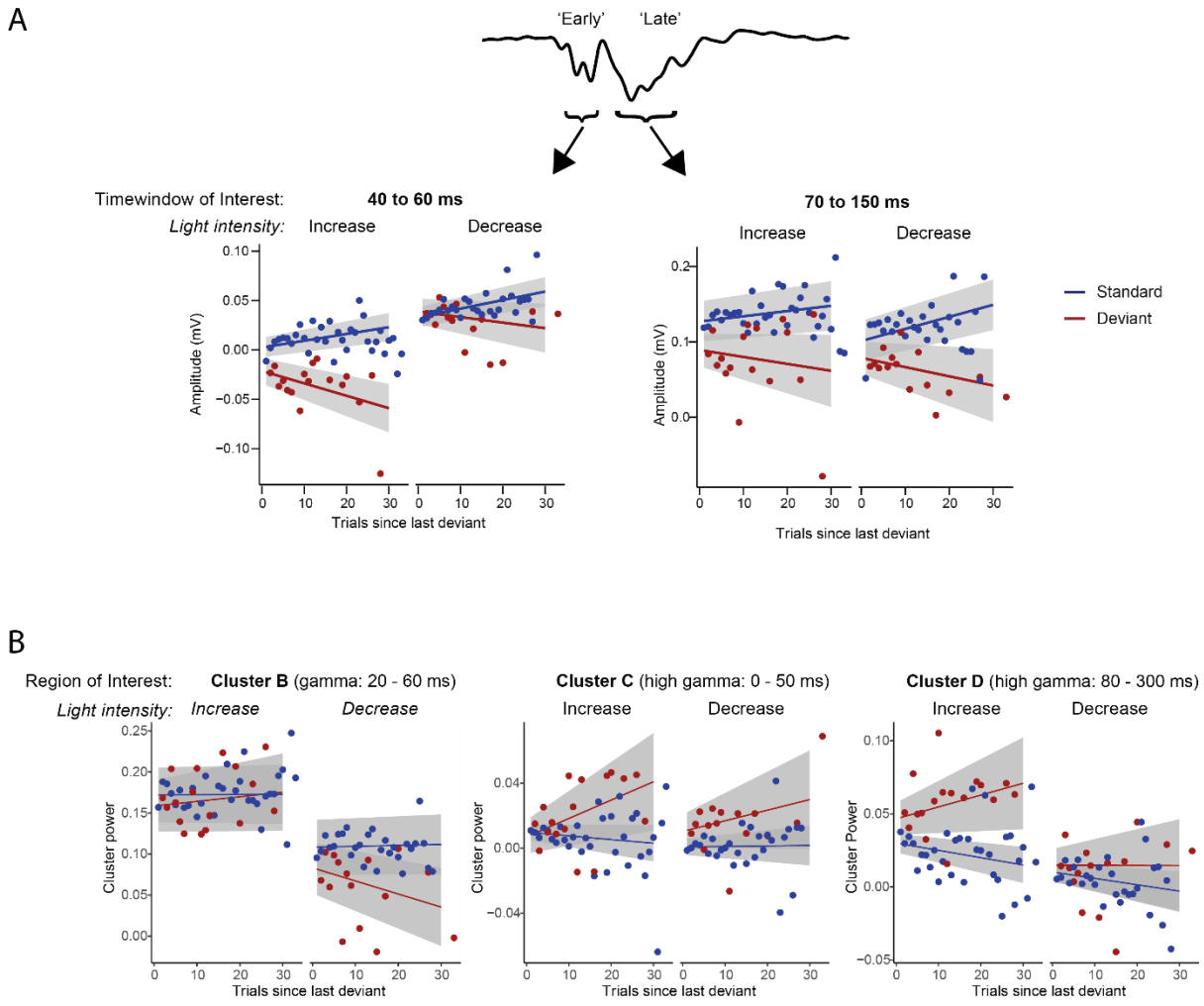

Figure 6. Exploration of effects of stimulus history on the various VEP- and TFR-based deviance detection features. Analyses were performed for the earlier found VEP **(A**, separated for the early and late negativity**)** and TFR **(B)** components. Each of the different graphs depicts the mean amplitude (for VEP features) or power (for TFR features) as a function of the number of preceding standards since the occurrence of the last deviant. The deviance detection amplitude is, for both VEP and TFR features, the difference between the standard and deviant amplitude, which was in some cases found to increase with an increasing number of preceding standards. Data are presented separately for standard and deviant stimuli, as well as for intensity increases and decreases. n = 13, data is presented as mean ± 95% confidence interval.

Early negativity (40-60 ms): the amplitude of the difference negativity (deviant minus standard) in the early latency increased with an increase in the number of trials since the last deviant, in other words an increase in the number of preceding standards (oddball ×

trials since last deviance: $F(1,25957)=24.6$, $p<0.0001$, Fig. 5A). Post-hoc analysis revealed that the increase in amplitudes of standard VEPs with increasing preceding standards was significant (t-ratio(13.9)=4.453, p=0.0006). Interestingly, the deviant amplitude was also affected, but decreased with a higher number of preceding standards (t-ratio(218.7)=2.549, p=0.0115). Furthermore, we confirmed our earlier observation that the amplitudes in the early latency window, irrespective of stimulus history, were stimulus specific (oddball × stimulus type: $F(1,25957)=22.1$, $p<0.0001$).

Late negativity (70-150 ms): amplitudes of the difference negativity in the late latency window paralleled the observations for the early component with respect to a modulation of the deviance detection by stimulus history (oddball × trials since last deviant: $F(1, 25958)=9.90$, $p=0.002$). However, post-hoc analysis revealed that while the increase of the amplitude of standard VEPs with decreasing novelty was also significant (t-ratio(14.2)=3.295, p=0.0052), contrary to the early latency, the deviant amplitude did not show a significant decrease in amplitude (t-ratio(270.9)=-1.544, p=0.1237). In this latency window no overall effect of stimulus type on deviant processing was observed (oddball × stimulus type: $F(1,25958=1.39$, $p=0.24$). To further address the stimulus independency, it was tested whether the effects of stimulus history on the late component differed between the stimulus types. Addition of this interaction to the model did not improve the fit of the model (ΔAIC=+2.1; ΔBIC=+26.4; a decrease indicating improvement of the model), supporting the claim that the amplitudes in the late component were indeed stimulus non-specific.

Oscillatory clusters: for the TRF-based analysis only the high gamma clusters (C and D, 80-150 Hz) showed a trend-significant relationship between stimulus history and deviance detection (C: oddball × trials since last deviant: $F(1, 25980)=4.18$, $p=0.04$; D: oddball ×

trials since last deviant: $F(1, 25980)=2.94$, $p=0.09$, Fig. 5B). However, the large variation and p-values close to the significance threshold suggest that these analyses were underpowered and therefore should be interpreted carefully.

4. Discussion

Deviance detection is an important function of the brain to identify environmental changes that may require subsequent appropriate behavioural and/or physiological responses. The goal of this study was to develop and validate a method for assessing visual deviance detection in freely behaving mice. The developed paradigm met all three pre-defined criteria: *a robust deviance response, stimulus-independence,* and *repeatability. First*, the light intensity-based oddball paradigm evoked a bi-phasic negativity in the VEP difference wave, of which the late 70-150 ms component was significantly different from zero, indicating that the paradigm was able to assess the ability of mice to differentiate between standard and deviant flashing light stimuli. *Second*, deviance detection in this late component was found to be independent of the type of stimulus (i.e., light increase or decrease) that was used a deviant. *Third*, the paradigm showed good repeatability in a second recording performed on a separate day.

The visual deviance detection presented with our paradigm matches well with previously reported visual deviance detection in both human and rodent EEG. The only other EEG-based visual deviance detection study in mice, in which a pattern-based oddball paradigm was used in head-fixed animals, also showed bi-phasic responses (Hamm and Yuste, 2016). They identified the differences in response to standard and deviant stimuli in early latencies to reflect stimulus-specific adaptation, while differences in later latencies reflected deviance detection activity. Also human visual ERP studies

530 indicated that early components of sensory processing represented adaptation effects,
531 while later components were specifically associated with violations of expectation
532 (Czigler et al., 2006; File et al., 2017). The onset and timing of the early and late phases
533 differed for each of the studies, as well as the present study, both between and within
534 species. Besides differences in neuronal pathways between species, deviance detection
535 latencies may also be influenced by the stimulus complexity (Kojouharova et al., 2019).
536 For example, Hamm and Yuste (2016), which used visual pattern stimuli instead of the
537 light flashes used in our study, found longer latencies (between ~ 40 and 240 ms) in their
538 mouse visual deviance detection features compared to the latencies observed in our
539 paradigm. In our freely-moving deviance detection paradigm, we could not assess the
540 contribution of stimulus-specific adaptation, as the 'many standards control paradigm'
541 (Czigler et al., 2006; Hamm and Yuste, 2016; Harms et al., 2016; File et al., 2017) was not
542 used. We were however able to show that the early component was sensitive to stimulus
543 properties (i.e. a larger deviance detection effect for light intensity increases), while the
544 late component was stimulus-type-independent. Taken together, our visual deviance
545 detection matches well with that observed in human as well as in mice. Our data show
546 that head fixation is not required for measuring visual deviance detection in mice, and
547 that the implemented paradigm and observed responses in mice have translational value.

548 Exploratory analysis of the effect of stimulus history showed that an increased
549 number of trials since the last deviant, in other words a longer stretch of preceding
550 standard presentations, increased the amplitude of the deviance detection. This was the
551 result of an increased amplitude of standard VEP responses and a decreased amplitude
552 of deviant VEP responses with a higher number of preceding standards. These changes
553 seem to suggest that our VEP-based deviance detection paradigm was sensitive to how
554 deviant a deviant stimulus is; as it showed larger responses when the previous deviant

was presented a longer time ago. The observed positive relationship between deviance detection amplitude and number of preceding standards could be a result of stimulus-specific adaptation of the standard, in our paradigm leading to increased amplitudes after more repetitions. However, larger deviance detection after more preceding standards could also result from the brain's response to the violation of a stronger memory-based expectation of the standard (Garrido et al., 2009). Although counterintuitive, violation-alerting activity in our data would actually be represented by the observed reduction in deviant amplitude, resulting in an increased difference with a standard. Further studies are needed to determine which of these two processes primarily drives the deviance detection features in our paradigm.

Larger differences in responses to standard and deviant visual pattern stimuli with more preceding standards have previously also been shown in rats, although this difference was dominantly driven by alterations in the responses to the deviant without a change in responses to the standard (Vinken et al., 2017). Also in human auditory MMN paradigms the amplitude of the MMN increases when the overall probability of deviants is decreased from 30% to 10% or from 13% to 1.5% (Sato et al., 2000; Sabri and Campbell, 2001), as well as with a higher number of standards preceding a deviant within a paradigm with a stable overall deviant probability of 20% (Matuoka et al., 2006). Together, these findings suggest that the effect size of our deviant detection paradigm could be further increased by having a higher minimum number of standards between deviants than the two currently used in our experiments.

In addition to the VEP waveforms, deviance detection was also found to be represented in both evoked and induced oscillatory activity. Human visual and mouse auditory studies have previously shown oscillatory responses related to deviance

579 detection, but the paradigms and corresponding responses showed large variability
580 (Stothart and Kazanina, 2013; Ahnaou et al., 2017; Hesse et al., 2017; Yan et al., 2017).
581 Differences across paradigms and species, as well as the fact that some of these studies
582 use auditory while others use visual stimuli, make a direct comparison of findings from
583 the studies assessing frequency response in deviance detection paradigms difficult.

584 In the TFR the higher gamma clusters between 50-150 Hz represented induced
585 (i.e. non-phase-locked) oscillatory activity. This is in line with the fact that induced power,
586 thought to represent top-down connections, concerns higher frequencies over longer
587 latencies, while evoked power, thought to represent bottom-up connections, concerns
588 lower frequencies over shorter latencies (Chen et al., 2012). The broad increase in high
589 gamma power (80-150 Hz) showed a tendency to be enhanced with more preceding
590 standards, although this effect was not statistically significant. Gamma frequency cortical
591 activity has generally been linked to increased spiking activity and network excitation
592 (Yizhar et al., 2011; Cho et al., 2015; Vogt et al,. 2015). In the visual cortex of freely
593 behaving mice, 30-100 Hz broadband gamma activity was found to functionally
594 discriminate between segregated cortical layers of visual processing (Senzai et al., 2019).
595 It was showed that gamma activity can be subdivided into functionally distinct broad-
596 (30-90 Hz) and narrowband (60 Hz) gamma oscillations, which show complementary
597 responses to changes in visual contrast (Saleem et al., 2017). While narrowband gamma
598 has been associated with thalamocortical communication, broadband gamma power is
599 thought to represent corticocortical communication. Although our recordings did not
600 allow to distinguish between underlying network mechanisms, the broad increase in high
601 gamma band activity we observed in the TFR deviant minus standard difference plots
602 could reflect increased corticocortical network activity during deviance processing. This
603 could suggest involvement of the prefrontal cortex, in line with what was found in human

visual deviance detection studies (Yucel et al., 2007; Kimura et al., 2010; Kimura et al., 2011), although no robust visual evoked responses were recorded from our prefrontal cortex electrode. The presence of induced broadband gamma responses thus seems to suggest communication between the visual cortex and other cortical areas during visual deviance detection. Whether this concerns frontal cortical areas remains to be studied.

In conclusion, we developed the first, robust and repeatable visual deviance detection paradigm based on changes in light intensity in freely behaving mice. Our paradigm provides a functional outcome measure for visual processing in these mice. Because no head fixation is needed, our paradigm minimizes animal discomfort while increasing behavioural relevance. The paradigm can easily be implemented to assess sensory processing deficits in mouse models of brain disease, and has the possibility to be compared with experiments in humans which increases translatability of preclinical outcomes.

Acknowledgements

This work was supported by a ZonMW TOP [grant number 91216021, 2017, awarded to HB and MJK] and the national Medical NeuroDelta [awarded to AvdM].

Declaration of interest

None

Author contribution statement

Renate Kat: Conceptualization, methodology, investigation, formal analysis, visualization, writing – original draft **Berry van der Berg:** Formal analysis, visualization, writing – reviewing & editing **Matthijs JL Perenboom:** Methodology, software **Maarten Schenke:** Investigation **Arn MJM van den Maagdenberg:** Resources, funding acquisition, writing – review & editting **Hilgo Bruining:** Funding aquisition, writing – review & editting **Else A Tolner:** Conceptualization, writing – reviewing & editting, supervision **Martien JH Kas:** Conceptualization, funding aquisition, writing – reviewing & editting, supervision

References

Ahnaou, A., Moechars, D., Raeymaekers, L., Biermans, R., Manyakov, N. V., Bottelbergs, A., Wintmolders, C., Van Kolen, K., Van De Casteele, T., Kemp, J.A., Drinkenburg, W.H., 2017. Emergence of early alterations in network oscillations and functional connectivity in a tau seeding mouse model of Alzheimer's disease pathology. Sci. Rep. 7, 1–14. https://doi.org/10.1038/s41598-017-13839-6

Baker, M., 2013. Neuroscience: Through the eyes of a mouse. Nature 502, 156–158. https://doi.org/10.1038/502156a

Bates, D., Maechler, M., Bolker, B., Walker, S., 2015. Package lme4. J. Stat. Softw. 67, 1–91. https://doi.org/http://lme4.r-forge.r-project.org

Carrillo-Reid, L., Han, S., Yang, W., Akrouh, A., Yuste, R., 2019. Controlling Visually Guided Behavior by Holographic Recalling of Cortical Ensembles. Cell 178, 447-457.e5. https://doi.org/10.1016/j.cell.2019.05.045

649 Chen, C.C., Kiebel, S.J., Kilner, J.M., Ward, N.S., Stephan, K.E., Wang, W.J., Friston, K.J.,
650 2012. A dynamic causal model for evoked and induced responses. Neuroimage 59,
651 340–348. https://doi.org/10.1016/j.neuroimage.2011.07.066

652 Cho, K.K.A., Hoch, R., Lee, A.T., Patel, T., Rubenstein, J.L.R., Sohal, V.S., 2015. Gamma
653 rhythms link prefrontal interneuron dysfunction with cognitive inflexibility in
654 dlx5/6+/- mice. Neuron 85, 1332–1343.
655 https://doi.org/10.1016/j.neuron.2015.02.019

656 Czigler, I., Weisz, J., Winkler, I., 2006. ERPs and deviance detection: Visual mismatch
657 negativity to repeated visual stimuli. Neurosci. Lett. 401, 178–182.
658 https://doi.org/10.1016/j.neulet.2006.03.018

659 File, D., File, B., Bodnár, F., Sulykos, I., Kecskés-Kovács, K., Czigler, I., 2017. Visual
660 mismatch negativity (vMMN) for low- and high-level deviances: A control study.
661 Attention, Perception, Psychophys. 79, 2153–2170.
662 https://doi.org/10.3758/s13414-017-1373-y

663 Fournier, J., Saleem, A.B., Diamanti, E.M., Wells, M.J., Harris, K.D., Carandini, M., 2020.
664 Mouse Visual Cortex Is Modulated by Distance Traveled and by Theta Oscillations.
665 Curr. Biol. 30, 3811-3817.e6. https://doi.org/10.1016/j.cub.2020.07.006

666 Garrido, M.I., Kilner, J.M., Stephan, K.E., Friston, K.J., 2009. The mismatch negativity: A
667 review of underlying mechanisms. Clin. Neurophysiol. 120, 453–463.
668 https://doi.org/10.1016/j.clinph.2008.11.029

669 Grimm, S., Escera, C., Nelken, I., 2016. Early indices of deviance detection in humans and
670 animal models. Biol. Psychol. 116, 23–27.
671 https://doi.org/10.1016/j.biopsycho.2015.11.017

672 Hamm, J.P., Shymkiv, Y., Mukai, J., Gogos, J.A., Yuste, R., 2020. Aberrant Cortical
673 Ensembles and Schizophrenia-like Sensory Phenotypes in Setd1a+/− Mice. Biol.
674 Psychiatry 88, 215–223. https://doi.org/10.1016/j.biopsych.2020.01.004

675 Hamm, J.P., Yuste, R., 2016. Somatostatin Interneurons Control a Key Component of
676 Mismatch Negativity in Mouse Visual Cortex. Cell Rep. 16, 597–604.
677 https://doi.org/10.1016/j.celrep.2016.06.037

678 Harms, L., Michie, P.T., Näätänen, R., 2016. Criteria for determining whether mismatch
679 responses exist in animal models: Focus on rodents. Biol. Psychol. 116, 28–35.
680 https://doi.org/10.1016/j.biopsycho.2015.07.006

681 Hesse, P.N., Schmitt, C., Klingenhoefer, S., Bremmer, F., 2017. Preattentive processing of
682 numerical visual information. Front. Hum. Neurosci. 11, 1–14.
683 https://doi.org/10.3389/fnhum.2017.00070

684 Hubel, D., Wiesel, T., 1968. Receptive Fields and Functional Architecture of Monkey
685 Striate Cortex. J. Physiol. 195, 215–243.
686 https://doi.org/10.1113/jphysiol.1968.sp008455

687 Hubel, D.H., 1959. Single unit activity in striate cortex of unrestrained cats. J. Physiol.
688 147, 226–238. https://doi.org/10.1113/jphysiol.1959.sp006238

689 Jones, S.R., 2016. When brain rhythms aren't 'rhythmic': implication for their
690 mechanisms and meaning. Curr. Opin. Neurobiol. 40, 72–80.
691 https://doi.org/10.1016/j.conb.2016.06.010

692 Kimura, M., 2012. Visual mismatch negativity and unintentional temporal-context-based
693 prediction in vision. Int. J. Psychophysiol. 83, 144–155.
694 https://doi.org/10.1016/j.ijpsycho.2011.11.010

695 Kimura, M., Kondo, H., Ohira, H., Schröger, E., 2011. Unintentional temporal context-
696 based prediction of emotional faces: An electrophysiological study. Cereb. Cortex
697 22, 1774–1785. https://doi.org/10.1093/cercor/bhr244

698 Kimura, M., Ohira, H., Schröger, E., 2010a. Localizing sensory and cognitive systems for
699 pre-attentive visual deviance detection: An sLORETA analysis of the data of Kimura
700 et al. (2009). Neurosci. Lett. 485, 198–203.
701 https://doi.org/10.1016/j.neulet.2010.09.011

702 Kimura, M., Widmann, A., Schröger, E., 2010b. Human visual system automatically
703 represents large-scale sequential regularities. Brain Res. 1317, 165–179.
704 https://doi.org/10.1016/j.brainres.2009.12.076

705 Kojouharova, P., File, D., Sulykos, I., Czigler, I., 2019. Visual mismatch negativity and
706 stimulus-specific adaptation: the role of stimulus complexity. Exp. Brain Res. 237,
707 1179–1194. https://doi.org/10.1007/s00221-019-05494-2

708 Kriegeskorte, N., Simmons, W.K., Bellgowan, P.S., Baker, C.I., 2009. Circular analysis in
709 systems neuroscience: The dangers of double dipping. Nat. Neurosci. 12, 535–540.
710 https://doi.org/10.1038/nn.2303

711 Kuznetsova, A., Brockhoff, P.B., Christensen, R.H.B., 2017. lmerTest Package: Tests in
712 Linear Mixed Effects Models. J. Stat. Softw. 82, 1–26.
713 https://doi.org/10.18637/jss.v082.i13

714 Maris, E., Oostenveld, R., 2007. Nonparametric statistical testing of EEG- and MEG-data.
715 J. Neurosci. Methods 164, 177–190.
716 https://doi.org/10.1016/j.jneumeth.2007.03.024

717 Matuoka, T., Yabe, H., Shinozaki, N., Sato, Y., Hiruma, T., Ren, A., Hara, E., Kaneko, S.,

718 2006. The Development of Memory Trace Depending on the Number of the
719 Standard Stimuli. Clin. EEG Neurosci. 37, 223–229.
720 https://doi.org/10.1177/155005940603700312

721 Matuschek, H., Kliegl, R., Vasishth, S., Baayen, H., Bates, D., 2017. Balancing Type I error
722 and power in linear mixed models. J. Mem. Lang. 94, 305–315.
723 https://doi.org/10.1016/j.jml.2017.01.001

724 May, P., Tiitinen, H., Ilmoniemi, R.J., Nyman, G., Taylor, J.G., Näätänen, R., 1999.
725 Frequency change detection in human auditory cortex. J. Comput. Neurosci. 6, 99–
726 120. https://doi.org/10.1023/A:1008896417606

727 Montijn, J.S., Olcese, U., Pennartz, C.M.A., 2016. Visual stimulus detection correlates with
728 the consistency of temporal sequences within stereotyped events of V1 neuronal
729 population activity. J. Neurosci. 36, 8624–8640.
730 https://doi.org/10.1523/JNEUROSCI.0853-16.2016

731 Näätänen, R., Sussman, E.S., Salisbury, D., Shafer, V.L., 2014. Mismatch negativity (MMN)
732 as an index of cognitive dysfunction. Brain Topogr. 27, 451–466.
733 https://doi.org/10.1007/s10548-014-0374-6

734 Oostenveld, R., Fries, P., Maris, E., Schoffelen, J.M., 2011. FieldTrip: Open source software
735 for advanced analysis of MEG, EEG, and invasive electrophysiological data. Comput.
736 Intell. Neurosci. 2011. https://doi.org/10.1155/2011/156869

737 Park, J., van den Berg, B., Chiang, C., Woldorff, M.G., Brannon, E.M., 2018. Developmental
738 trajectory of neural specialization for letter and number visual processing. Dev. Sci.
739 21, 1–14. https://doi.org/10.1111/desc.12578

740 Perenboom, T., Schenke, M., Ferrari, M., Terwindt, G., van den Maagdenberg, A., Tolner,

741 E., 2020. Responsivity to light in familial hemiplegic migraine type 1 mutant mice
742 reveals frequency-dependent enhancement of visual network excitability. Eur. J.
743 Neurosci. 53, 1672–1686. https://doi.org/10.1111/ejn.15041

744 Sabri, M., Campbell, K.B., 2001. Effects of sequential and temporal probability of deviant
745 occurrence on mismatch negativity. Cogn. Brain Res. 12, 171–180.
746 https://doi.org/10.1016/S0926-6410(01)00026-X

747 Saleem, A.B., Lien, A.D., Krumin, M., Haider, B., Rosón, M.R., Ayaz, A., Reinhold, K., Busse,
748 L., Carandini, M., Harris, K.D., Carandini, M., 2017. Subcortical Source and
749 Modulation of the Narrowband Gamma Oscillation in Mouse Visual Cortex. Neuron
750 93, 315–322. https://doi.org/10.1016/j.neuron.2016.12.028

751 Sassenhagen, J., Draschkow, D., 2019. Cluster-based permutation tests of MEG/EEG data
752 do not establish significance of effect latency or location. Psychophysiology 56, 1–8.
753 https://doi.org/10.1111/psyp.13335

754 Sato, Y., Yabe, H., Hiruma, T., Sutoh, T., Shinozaki, N., Nashida, T., Kaneko, S., 2000. The
755 effect of deviant stimulus probability on the human mismatch process. Neuroreport
756 11, 3703–3708. https://doi.org/10.1097/00001756-200011270-00023

757 Sculthorpe, L.D., Ouellet, D.R., Campbell, K.B., 2009. MMN elicitation during natural sleep
758 to violations of an auditory pattern. Brain Res. 1290, 52–62.
759 https://doi.org/10.1016/j.brainres.2009.06.013

760 Senzai, Y., Fernandez-Ruiz, A., Buzsáki, G., 2019. Layer-Specific Physiological Features
761 and Interlaminar Interactions in the Primary Visual Cortex of the Mouse. Neuron
762 101, 500-513.e5. https://doi.org/10.1016/j.neuron.2018.12.009

763 Sohya, K., Kameyama, K., Yanagawa, Y., Obata, K., Tsumoto, T., 2007. GABAergic neurons

764 are less selective to stimulus orientation than excitatory neurons in layer II/III of
765 visual cortex, as revealed by in vivo functional Ca2+ imaging in transgenic mice. J.
766 Neurosci. 27, 2145–2149. https://doi.org/10.1523/JNEUROSCI.4641-06.2007

767 Stagg, C., Hindley, P., Tales, A., Butler, S., 2004. Visual mismatch negativity: the detection
768 of stimulus change. Neuroreport 15, 487–491.
769 https://doi.org/10.1097/01.wnr.00001

770 Stothart, G., Kazanina, N., 2013. Oscillatory characteristics of the visual mismatch
771 negativity; what evoked potentials aren't telling us. Front. Hum. Neurosci. 7, 1–9.
772 https://doi.org/10.3389/fnhum.2013.00426

773 Sulykos, I., Czigler, I., 2014. Visual mismatch negativity is sensitive to illusory brightness
774 changes. Brain Res. 1561, 48–59. https://doi.org/10.1016/j.brainres.2014.03.008

775 Tada, M., Kirihara, K., Mizutani, S., Uka, T., Kunii, N., Koshiyama, D., Fujioka, M., Usui, K.,
776 Nagai, T., Araki, T., Kasai, K., 2019. Mismatch negativity (MMN) as a tool for
777 translational investigations into early psychosis: A review. Int. J. Psychophysiol.
778 145, 5–14. https://doi.org/10.1016/j.ijpsycho.2019.02.009

779 Van Diepen, H.C., Ramkisoensing, A., Peirson, S.N., Foster, R.G., Meijer, J.H., 2013.
780 Irradiance encoding in the suprachiasmatic nuclei by rod and cone photoreceptors.
781 FASEB J. 27, 4204–4212. https://doi.org/10.1096/fj.13-233098

782 Vinken, K., Vogels, R., Op de Beeck, H., 2017. Recent Visual Experience Shapes Visual
783 Processing in Rats through Stimulus-Specific Adaptation and Response
784 Enhancement. Curr. Biol. 27, 914–919. https://doi.org/10.1016/j.cub.2017.02.024

785 Vogt, D., Cho, K.K.A., Lee, A.T., Sohal, V.S., Rubenstein, J.L.R., 2015. The
786 Parvalbumin/Somatostatin Ratio Is Increased in Pten Mutant Mice and by Human

PTEN ASD Alleles. Cell Rep. 11, 944–956. https://doi.org/10.1016/j.celrep.2015.04.019

Warden, M.R., Cardin, J.A., Deisseroth, K., 2014. Optical neural interfaces. Annu. Rev. Biomed. Eng. 16, 103–129. https://doi.org/10.1146/annurev-bioeng-071813-104733

Yan, T., Feng, Y., Liu, T., Wang, L., Mu, N., Dong, X., Liu, Z., Qin, T., Tang, X., Zhao, L., 2017. Theta oscillations related to orientation recognition in unattended condition: A vMMN study. Front. Behav. Neurosci. 11, 1–8. https://doi.org/10.3389/fnbeh.2017.00166

Yizhar, O., Fenno, L.E., Prigge, M., Schneider, F., Davidson, T.J., Shea, D.J.O., Sohal, V.S., Goshen, I., Finkelstein, J., Paz, J.T., Stehfest, K., Fudim, R., Ramakrishnan, C., Huguenard, J.R., Hegemann, P., Deisseroth, K., 2011. Neocortical excitation / inhibition balance in information processing and social dysfunction. Nature 477, 171–178. https://doi.org/10.1038/nature10360

Yucel, G., McCarthy, G., Belger, A., 2007. fMRI reveals that involuntary visual deviance processing is resource limited. Neuroimage 34, 1245–1252. https://doi.org/10.1016/j.neuroimage.2006.08.050

Zhang, D., Yu, B., Liu, J., Jiang, W., Xie, T., Zhang, R., Tong, D., Qiu, Z., Yao, H., 2017. Altered visual cortical processing in a mouse model of MECP2 duplication syndrome. Sci. Rep. 7, 1–14. https://doi.org/10.1038/s41598-017-06916-3

Supplementary Material

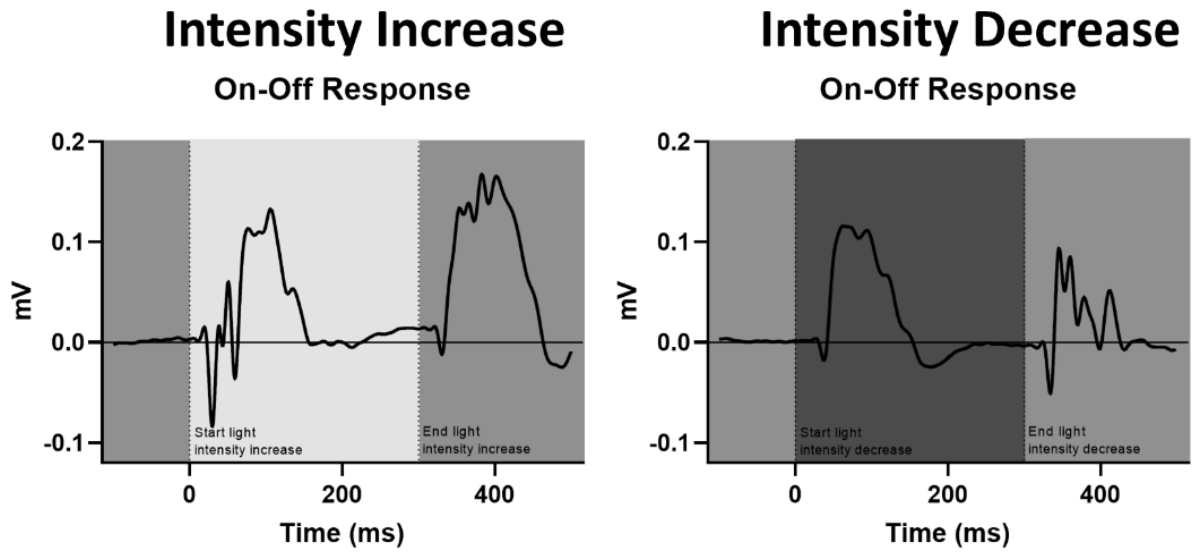

Figure S1. **Comparison of VEP waveforms for the On- and Off-responses to a light intensity increase versus light intensity decreases.** Light Stimuli lasted for 300 ms, whereby these plots show the 'On-response' to the start of the 300-ms intensity increase or decrease as well as the VEP 'Off-response' to the light intensity changing back to baseline level. The On-response of the light increase, as well as the Off-response of the light decrease, concern a response to an increase in light intensity. The On-response of the light decrease, as well as the Off-response of the light increase, concern a response to a light intensity decrease. Presented data show the responses to light increases and decreases, averaged for right and left V1 responses and the 2 recordings on separate days.